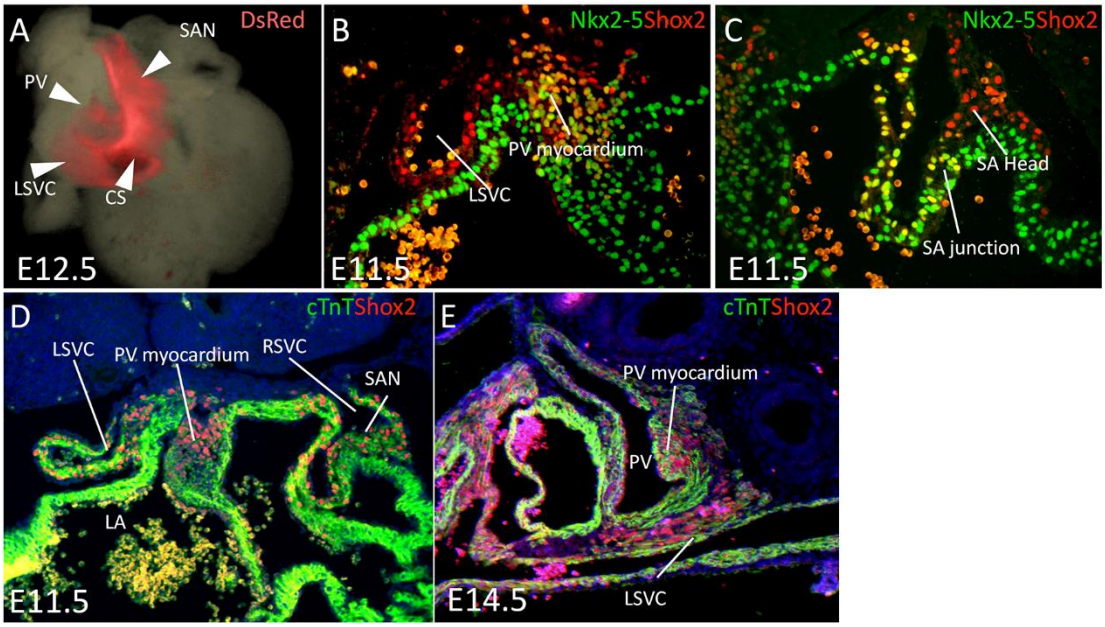


**Figure S1. Developmental expression of *Shox2* in the venous pole and PV myocardium.** (A-C) Expression of *Shox2* in the venous pole, as revealed by DsRed activity in an E12.5 *Shox2*$^{HA/+}$ embryo (A), and its co-localization with Nkx2-5, as detected by immunohistochemistry, in the PV and SAN of an E11.5 embryo (B,C). (D,E) Co-immunostaining of cTnT and Shox2 in the venous pole at E11.5 (D) and E14.5 (E). CS, coronary sinus; PV, pulmonary vein; SAN, sinoatrial node; LSVC, left superior vena cava; RSVC, right superior vena cava.

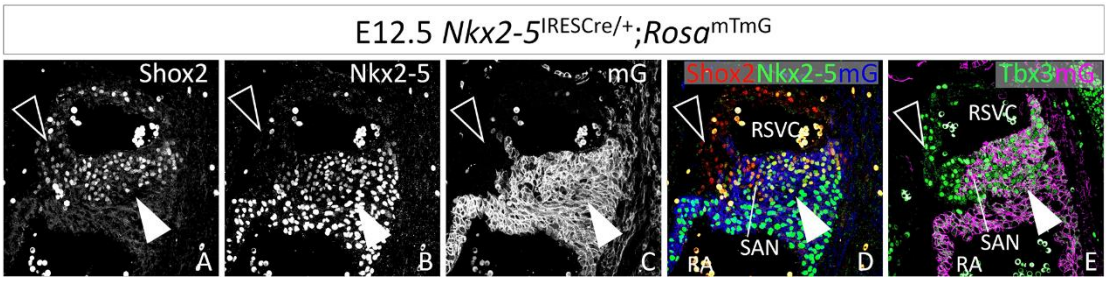


**Figure S2. Fate mapping of the SAN by *Nkx2-5*$^{IRESCre/+}$;*ROSA*$^{mTmG}$ mice at E12.5.** (A-E) Co-immunofluorescence of Shox2, Nkx2-5, membrane-bound GFP (mG) and Tbx3 confirmed the existence of the *Nkx2-5*$^{+}$ (arrowhead) and *Nkx2-5*$^{-}$ (open arrowhead) domains of the SAN.

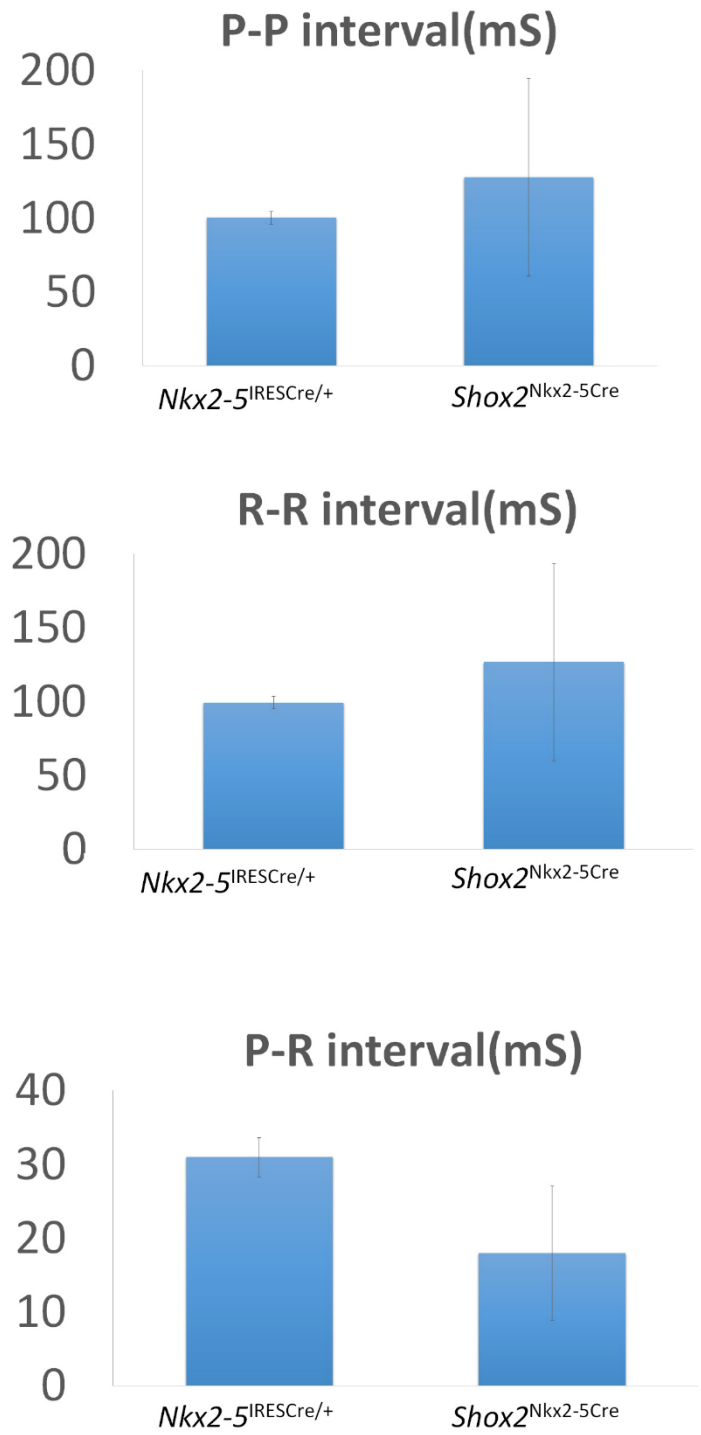


**Figure S3. Comparison of average P-P, R-R and P-R intervals in *Shox2*$^{Nkx2\text{-}5Cre}$ and control mice.** Histogram shows significantly variable P-P, R-R, and P-R intervals, determined by surface ECG, in *Shox2*$^{Nkx2\text{-}5Cre}$ mice, as compared to background and age matched controls.

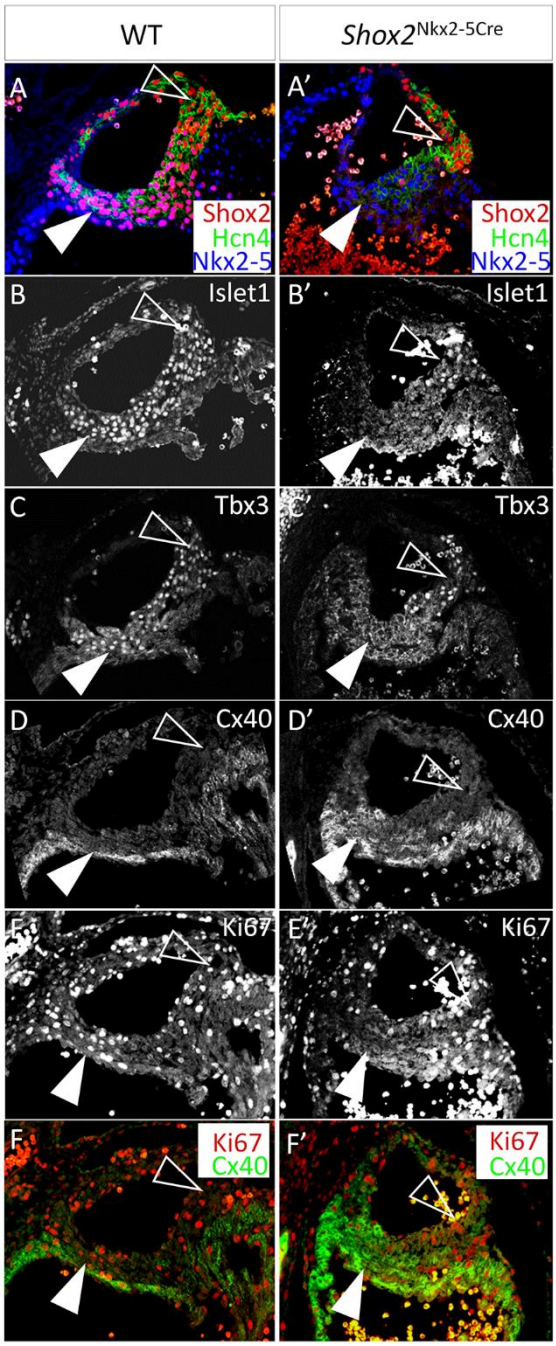


**Figure S4. Inactivation of *Shox2* in the *Nkx2-5*$^{+}$ domain leads to loss of SAN identity and reduced cell proliferation index.** (A-C') Tissue specific inactivation of *Shox2* in the *Nkx2-5*-expressing domain compromises the fate of SA junction cells, as revealed by loss of *Hcn4*, *Islet1*, and *Tbx3* expression in E12.5 *Shox2*$^{Nkx2\text{-}5Cre}$ mice (A', B', and C'), compared to controls (A, B, and C). (D-F') Cell proliferation index is

also reduced, shown by Ki67 staining, within the SA junction where *Cx40* is ectopically activated in *Shox2*$^{Nkx2\text{-}5Cre}$ embryos (D', E', and F'), compared to controls (D, E, and F). Open arrowheads point to the *Nkx2-5*$^{-}$ SAN head where gene expression and cell proliferation are unaffected in the mutants. Arrowheads point to the *Nkx2-5*$^{+}$ SA junction where cell proliferation index marker Ki67 is almost completely abolished and gene expression is altered.

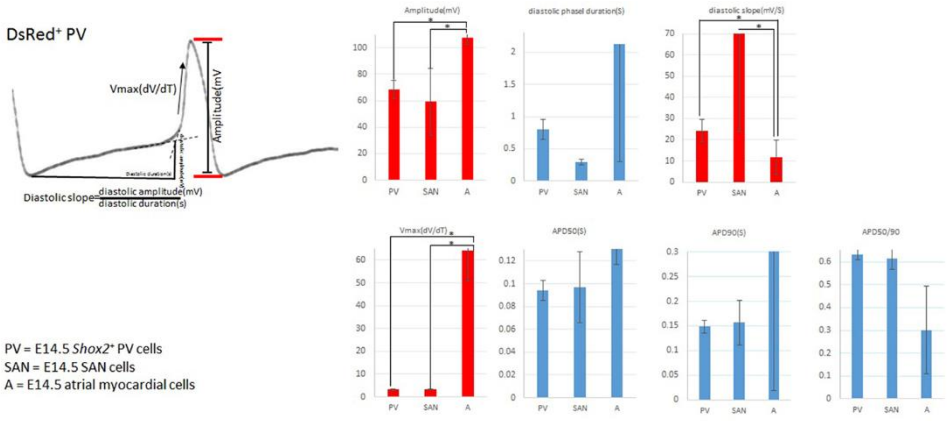


**Figure S5. Average action potential parameters of FACS isolated *Shox2*$^{+}$ PV cells in comparison with SAN and atrial myocardial cells.** Histograms show average action potential parameters of E14.5 *Shox2*$^{+}$ PV cells, SAN cells, and atrial myocardial cells. The red histograms highlight statistically significantly distinctive features of *Shox2*$^{+}$ PV cells and SAN cells as compared to atrial cells.

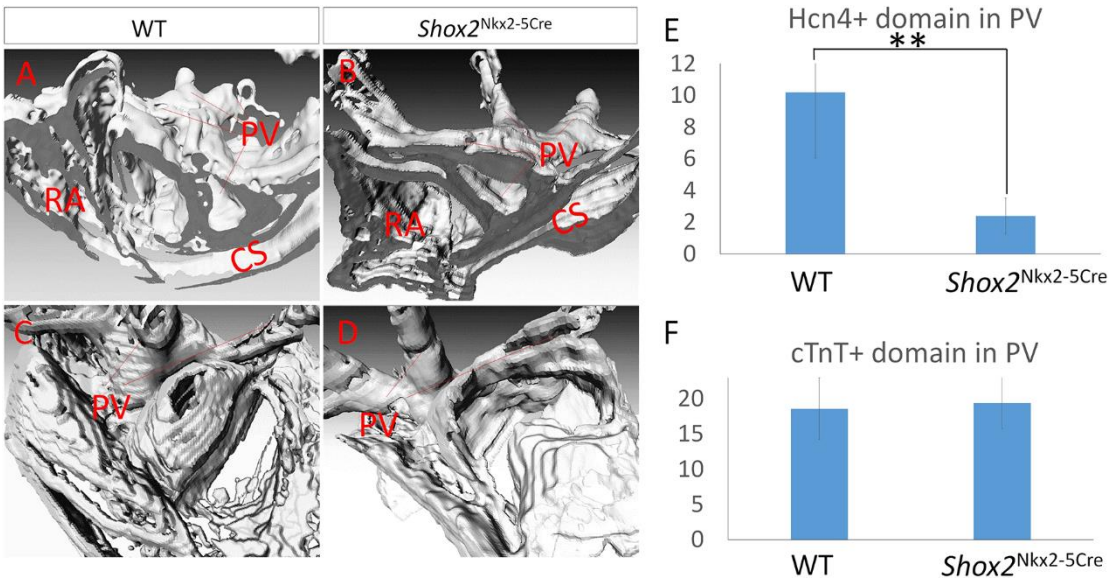


**Figure S6. Morphometric study of the *Nkx2-5*$^{IRESCre/+}$;*Shox2*$^{F/F}$ PV.** (A-D) 3-D reconstructions of the venous pole of E14.5wild type (A,C) and *Nkx2-5*$^{IRESCre/+}$;*Shox2*$^{F/F}$ (*Shox2*$^{Nkx2\text{-}5Cre}$) (B,D) mice. (E,F) Comparison of relative volumes of *Hcn4*$^{+}$ and *cTnT*$^{+}$ domains in the PV of E14.5 control (E) and mutant (F) mice.

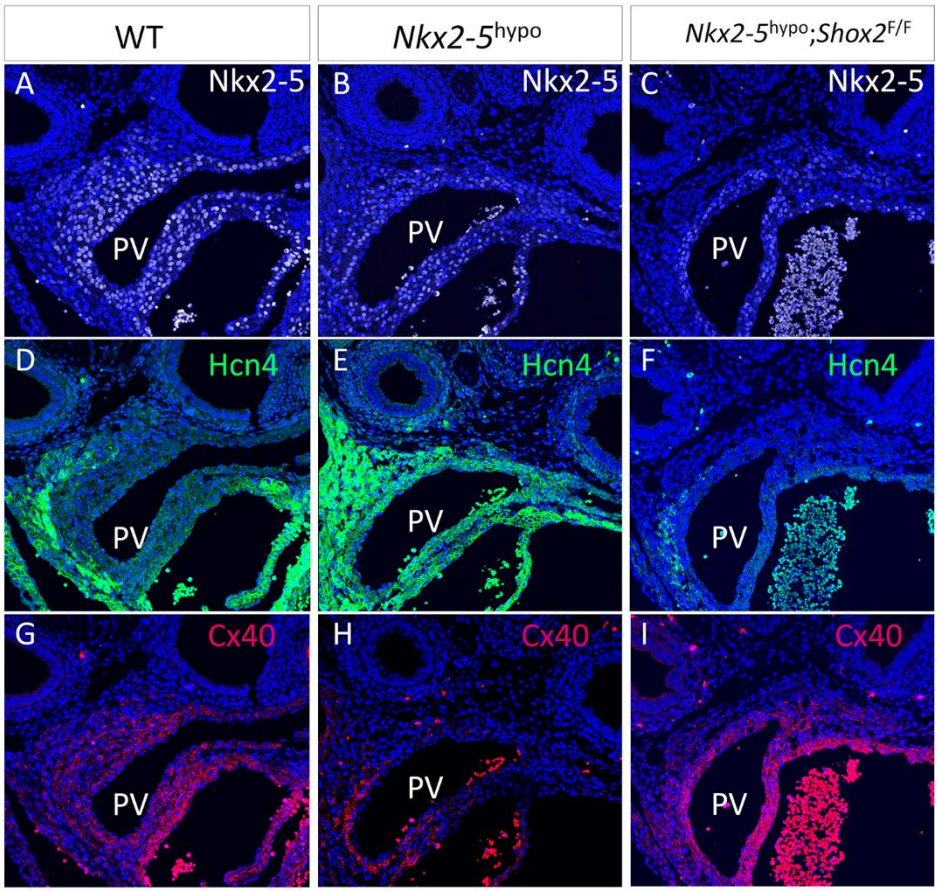


**Figure S7. Separate channel views of Figure 5 J-L'.** Comparison of Nkx2-5, Hcn4 and Cx40 expression in the PV myocardium of control (A,D,G), *Nkx2-5*$^{hypo}$ (B,E,H), and *Nkx2-5*$^{hypo}$;*Shox2*$^{F/F}$ mice (C,F,I).

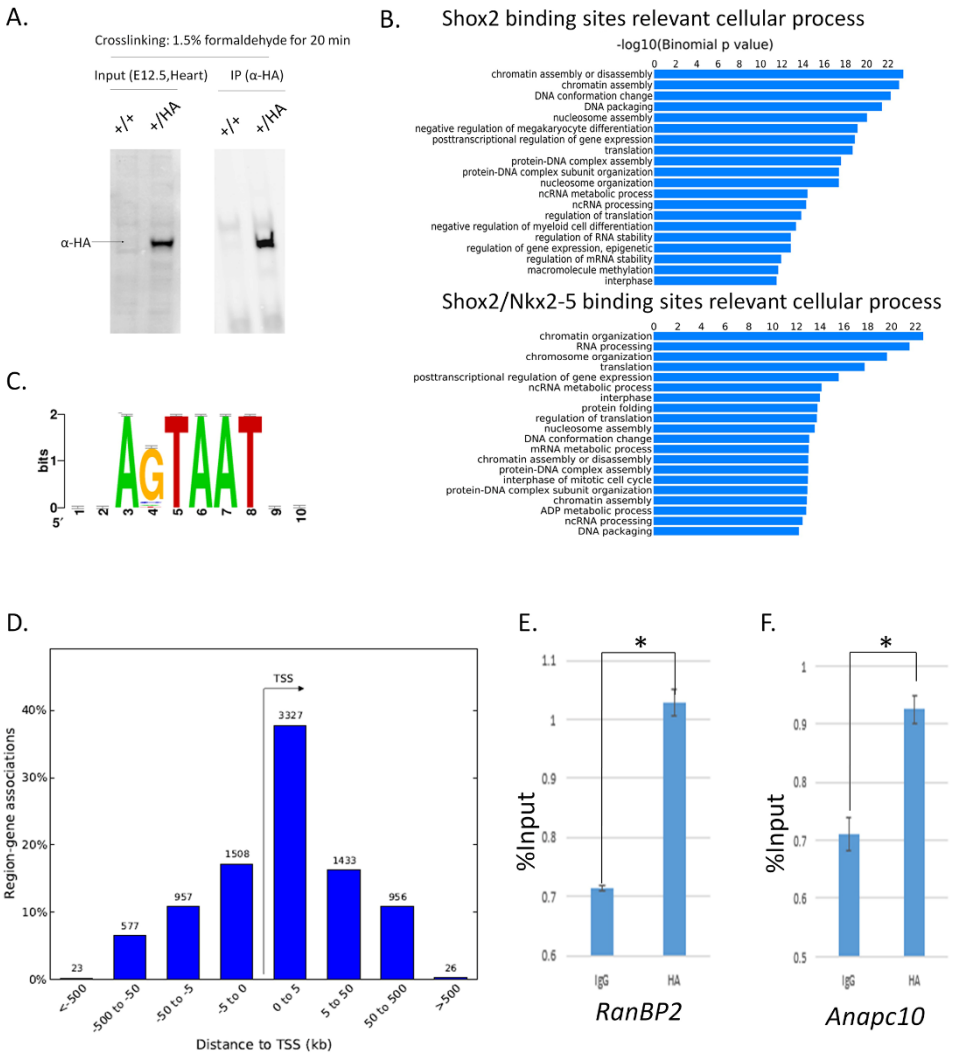


**Figure S8. Supplemental information for ChIP-Seq study on Shox2.** (A) Immunoprecipitation HA-tagged Shox2 protein by α-HA antibody after crosslinking. (B) Association of Shox2 binding sites and Shox2/Nkx2-5 binding sites with basic cellular processes. (C) Core motif of Shox2 binding sites discovered in 10% of top peaks. (D) Plotting of Shox2 binding sites around transcription start site (TSS). (E,F) Verification of Shox2 binding sites in *RanBP2* (E) and *Anapc10* (F) by in vivo ChIP assays on E12.5 embryonic *Shox2*$^{HA}$ hearts.

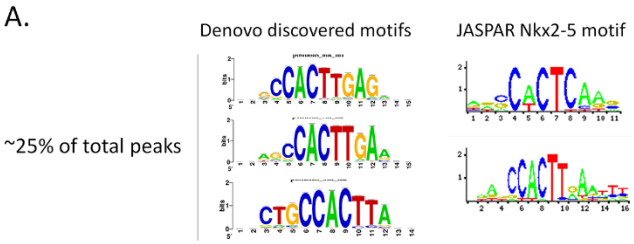


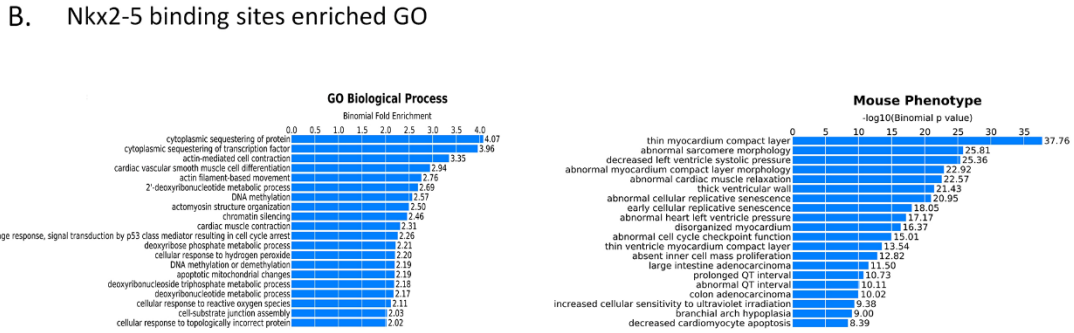


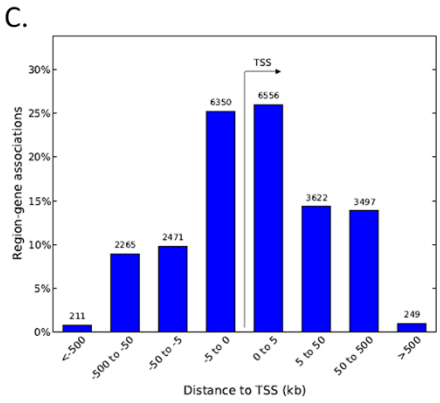


**Figure S9. Supplemental information for ChIP-Seq study on Nkx2-5.** (A) Comparison of de novo discovered Nkx2-5 motif to JASPAR Nkx2-5 motif. (B) Gene Ontology analysis of total Nkx2-5 binding sites. (C) Plotting of Nkx2-5 binding sites in relation to transcription start site (TSS).

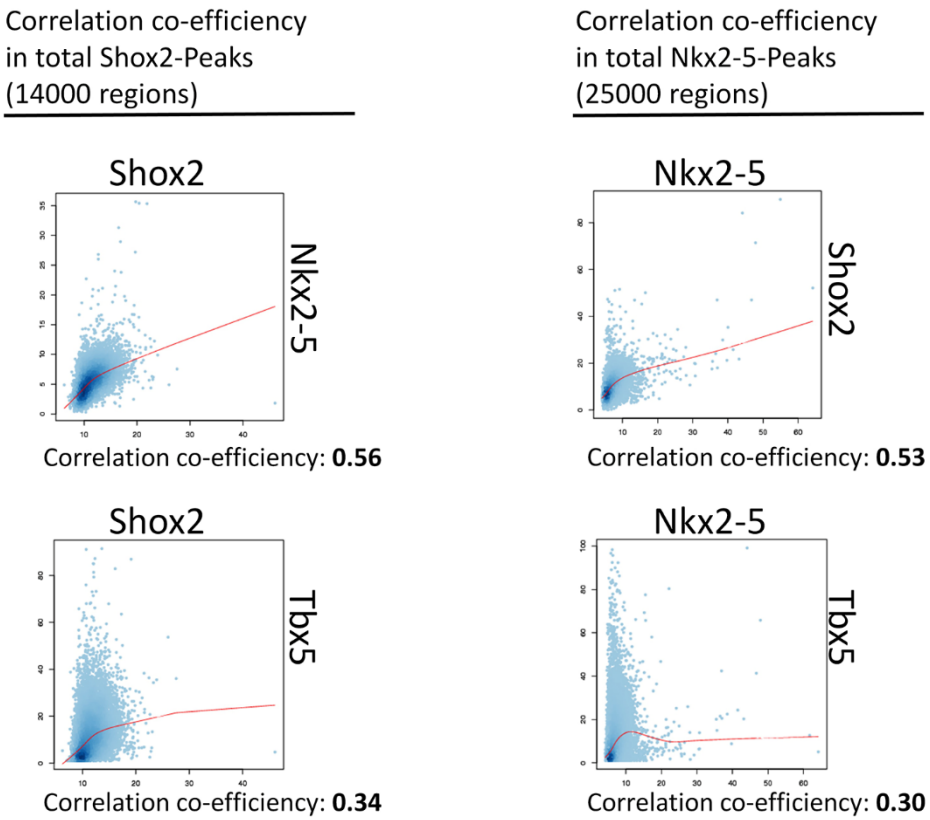


**Figure S10. Correlation co-efficiency.** As shown, correlation co-efficiency between genome coverage of ChIP samples in total Shox2 peak regions and total Nkx2-5 peak regions are calculated by multiple wiggle correlation (Liu et al., 2011) using bedgraphs of ChIP signal as input.

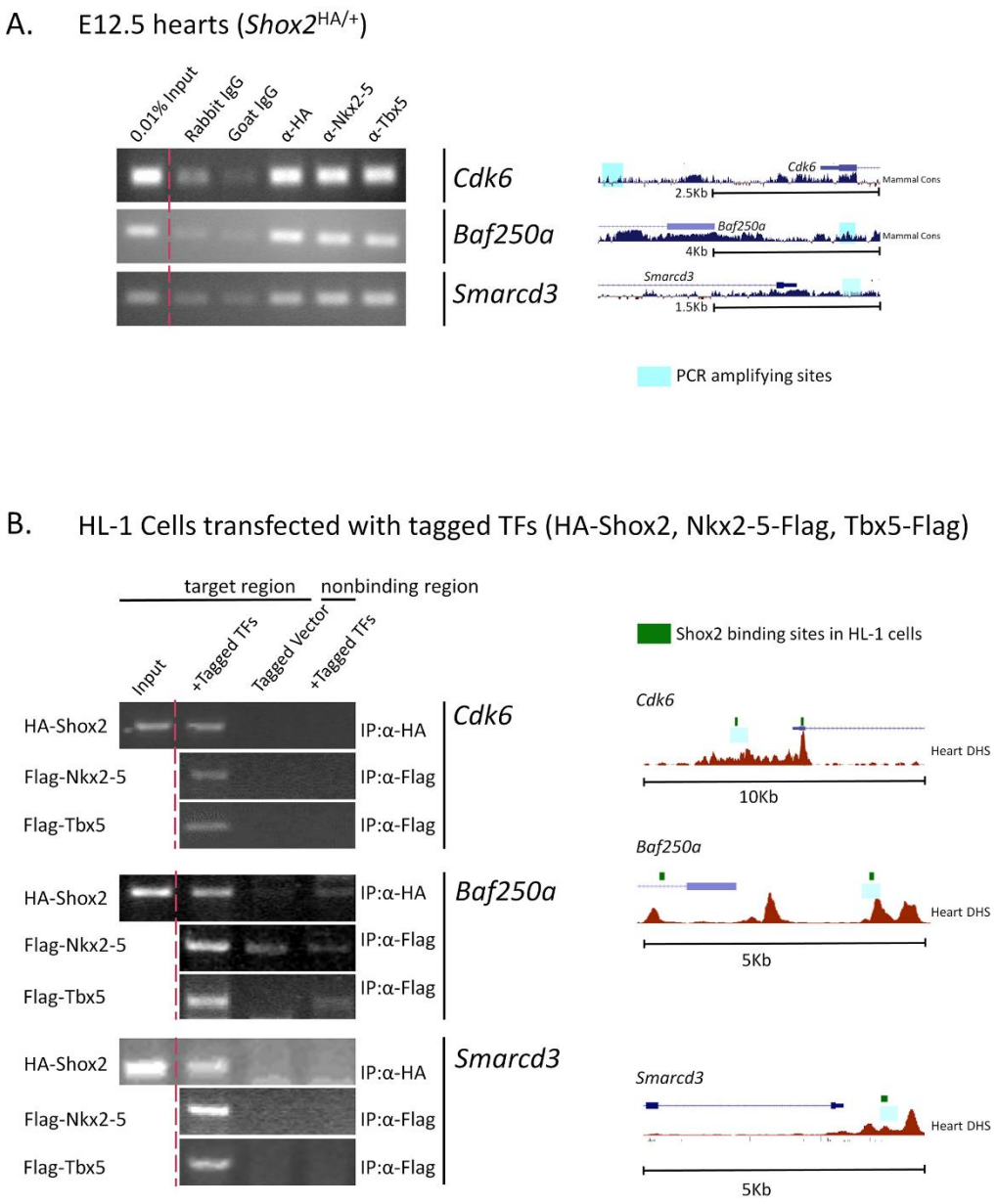


**Figure S11. ChIP-PCR confirms co-binding of Shox2, Nkx2-5, and Tbx5 in selected genes in embryonic heart and HL-1 cells.** (A) ChIP-PCR results show binding of Shox2, Nkx2-5, and Tbx5 on the same sites in the regulatory regions of Cdk6, Baf250a, and Smarcd3 genes in E12.5 hearts. (B) ChIP-PCR results demonstrate binding of these three factors on the same sites of the selected genes in HL-1 cells. Note that for ChIP-PCR in HL-1 cells, a small scale ChIP-Seq (Ion Torrent, Invitrogen) was performed to evaluate the normal binding behavior of Shox2.

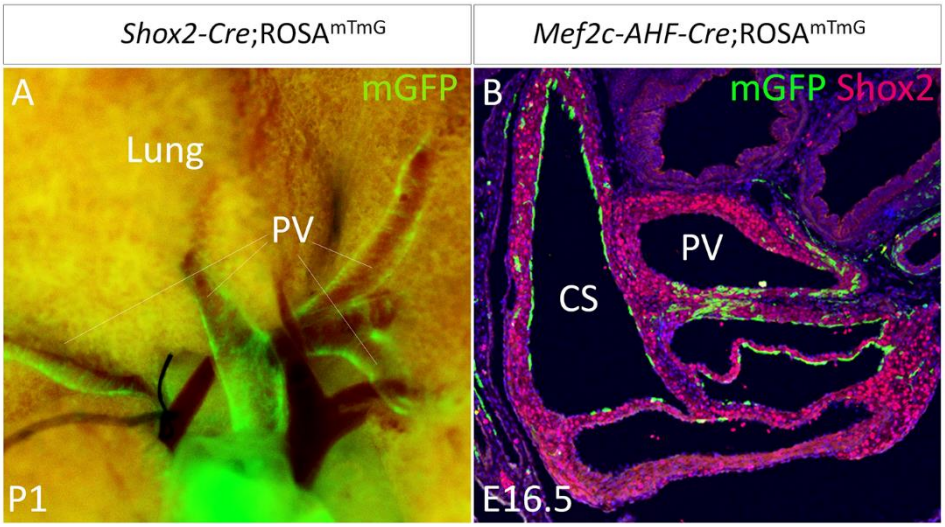


**Figure S12. Fate mapping of lineage composition of the PV.** (A) Fate mapping of the PV by *Shox2-Cre*;*ROSA*$^{mTmG}$ mice at postnatal day 1. (B) Contribution of the dorsal mesenchyme protrusion to the PV myocardium where *Shox2* is highly expressed is evaluated by lineage tracing in an E16.5 *Mef2c-AHF-Cre*;*ROSA*$^{mTmG}$ mice. CS, coronary sinus; PV, pulmonary vein.

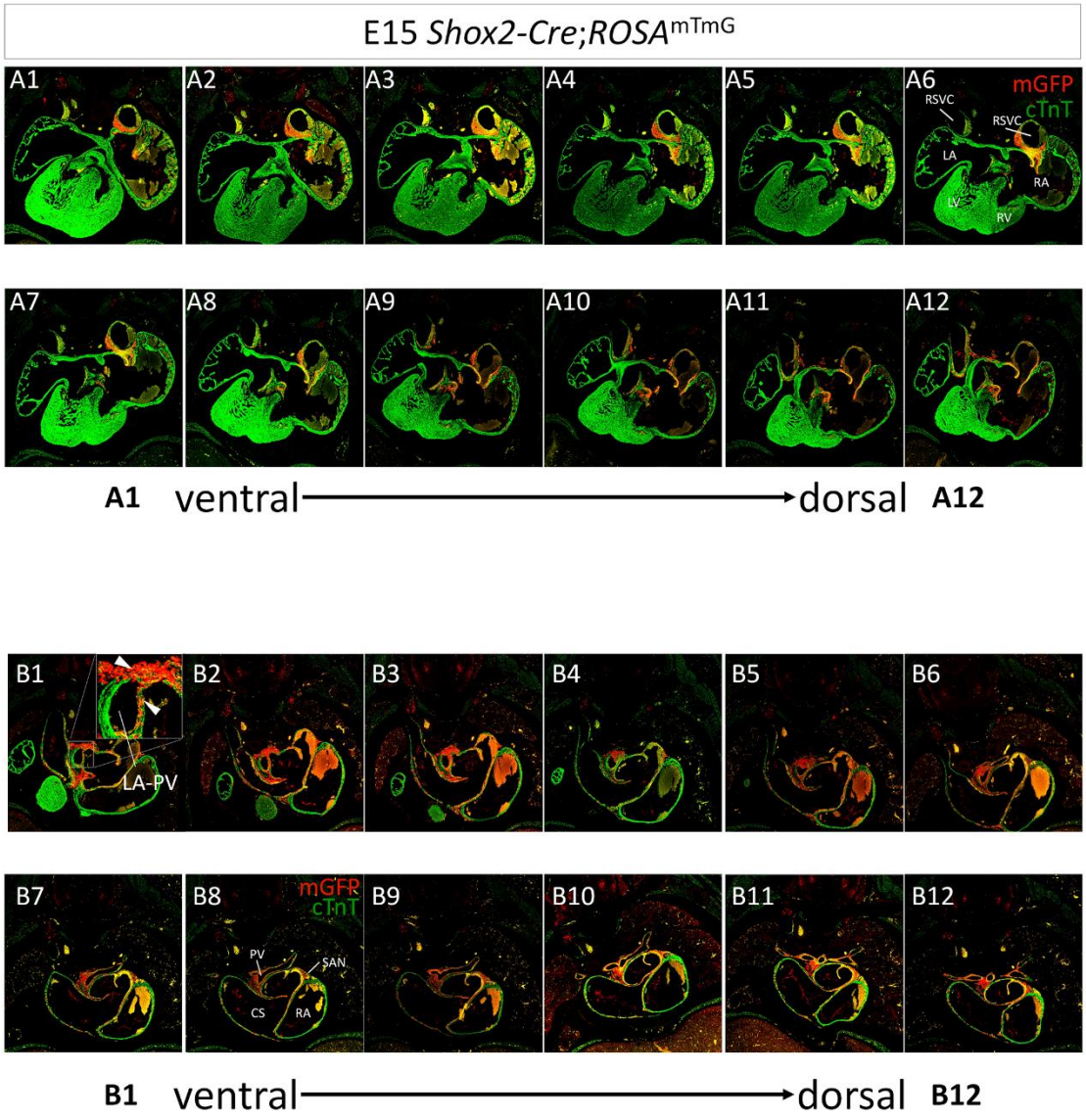


**Figure S13. Serial sections of *Shox2-Cre*;*ROSA*$^{mTmG}$ mice at E15.** The expression pattern of *Shox2* in myocardium is detailed by co-immunofluorescence of cTnT and mG around the SAN (A1-A12) and the PV (B1-B12) in serial sections (shown in every 20-μm). Arrowheads in B1 points to *Shox2* expression domain around the lumen where the PV opens into left atrium. A6 and B8 represent the orientations and section planes of the images presented in the current study to show the SAN and the PV, respectively. CS, coronary sinus; LA, left atrial; PV, pulmonary vein; RA, right atrial; SAN, sinoatrial node; LA-PV, transitional domain where the PV opens into left atrium; LSVC, left superior vena cava; RSVC, right superior vena cava.


**Figure S14. Verification of *Nkx2-5* siRNA efficacy.** Western blot assay demonstrates high efficacy of Nkx2-5 siRNA (Si-Nkx2-5) in HL-1 cells 72 hours after transfection, as compared with mock controls.

## Supplementary Methods

### Antibody information and working concentration

The primary antibodies used in this study were purchased and diluted in the blocking solution as detailed below: anti-HA (3F10, Roche; 1:1000), anti-Hcn4 (SHG1E5, Abcam; 1:1000), anti-Shox2 (homemade; 1:1000), anti-Nkx2-5 (N-19, Santa Cruz; 1:1000; ab35843, Abcam; 1:500), anti-Tbx3 (A-20, Santa Cruz; 1:500), anti-Cx40 (C-20, Santa Cruz; 1:1000), anti-Islet1 (ab20670, Abcam; 1:1000), anti-cardiac troponin T (Ab-1, Thermo Scientific; 1:5000), anti-Ki67 (D3B5, Cell Signaling; 1:300).

### Chromatin immunoprecipitation (ChIP) and ChIP-Seq

ChIP on E12.5 embryonic hearts from *Shox2*$^{HA}$ mice and on transfected HL-1 cells was performed using Active Motif HS ChIP Kit following manufacturer's protocol using α-HA for HA-Shox2 (ab9110, abcam), Anti-Nkx2-5 (N-19, Santa Cruz ) and anti-Tbx5 (AB1, Sigma). ChIP purified DNAs were subjected to ChIP-PCR or ChIP-Sequencing. Library construction and sequencing were performed at Active Motif (Carlsbad, CA) and BGI (Hong Kong, China). For Shox2 ChIP, two independently collected ChIP DNAs (sequenced by HiSeq2000, Illumine) were combined to generate ~65 million mapped reads after removing duplication reads for ChIP reaction and ~55 million mapped reads for input reaction. For Nkx2-5 ChIP, ~30 million mapped reads were generated for ChIP reaction and ~30 million mapped reads for input reaction were generated and used for subsequent analysis. Peak calling and subsequent analysis of Shox2, Nkx2-5, and Tbx5 (He et al., 2011) ChIP reads were done by MACS.version2 (Zhang et al., 2008) ($10^{-5}$ cutoff) and BED tools inserted in the galaxy project main instance and galaxy cistrome instance. Peaks coincide with the sequencing blacklist (Consortium, 2012) that often represents artificial signals

were removed from the analysis. Motif discovery was done by MEME Suite (Bailey et al., 2009) and RSAT (Thomas-Chollier et al., 2011). Primer sequences for ChIP qPCR will be available upon request.

**Differentiation of embryoid bodies and siRNA treatment.**

About 500-1000 ES cells were placed in each well of 96-well ultralow attachment plate. Ten-day after in culture at which time differentiated EBs showed consistent spontaneous beats, an indication of cardiomycyte differentiation, EBs were harvested and fixed in 4% PFA, paraffin embedded, and subjected to sectioning and immunofluorescence analysis. For siRNA treatment, EBs were dissociated into small cell clumps by brief treatment with collagenase and allowed to attach onto gelatin-coated plates. 16-hr after in culture, cells were transfected by scramble RNA (Ambion) or *Nkx2-5* siRNA pool (siGenome, Dharmacon) by RNAiMax (Life-Technologies) for 72-hr prior to harvest and analysis. The efficiency of siRNA was determined in HL-1 cells (Claycomb et al., 1998) that express a high level of *Nkx2-5* (supplementary material Fig. S14). Standard qPCR and normalization were described previously (Yang et al., 2014). Primers for *Hcn4* transcripts are 5'-GATTATCCACCCCTACAGTGAC-3' (F) and 5'-ACCACATTGAAGACGATCCAG-3' (R).

**Recording of action potential**

The DsRed$^{+}$ proximal PV domain was dissected out from E14.5 *Shox2*$^{HA}$ embryos under fluorescent dissecting scope, and subjected to digestion by a cocktail of collagenase I, II, IV, followed by brief trypsin treatment. Suspended cells were subjected to FACS. DsRed$^{+}$ cells were allowed to attach onto fibronectin-gelatin

coated coverslips and recover overnight before whole-cell patch recordings were performed under 36.0±0.5$^0$C in an extracellular solution that contained NaCl (140-mM), KCl (5.4-mM), $CaCl_2$ (1.8-mM), $MgCl_2$ (1.0-mM), glucose (5.5-mM), and HEPES (5.0-mM) at pH7.4 and internal solution containing KGlu (120-mM), KCl (20-mM),-NaCl (4-mM), HEPES (10-mM), EGTA (0.2-mM), Mg-ATP (4-mM), $Na_2$-phosphocreatinine (14-mM), and Tris-GTP (0.3-mM) at pH7.2. The configurations of action potentials were analyzed by Clampfit 10.5 (Molecular Devices, LLC).

### 3D reconstruction

For 3D reconstruction, consecutive 10-μm sections were stained by α-cTnT or α-Hcn4 antibodies, imaged, and loaded into Amira 5.4 (FEI Visualization Sciences Group). Subsequent alignment, segmentation, and 3D model generation were performed according to the help document provided by FEI Visualization Sciences Group.

## Supplementary References

**Bailey, T. L., Boden, M., Buske, F. A., Frith, M., Grant, C. E., Clementi, L., Ren, J., Li, W. W. and Noble, W. S.** (2009). MEME SUITE: tools for motif discovery and searching. *Nucleic acids research* **37**, W202-208.

**Claycomb, W. C., Lanson, N. A., Jr., Stallworth, B. S., Egeland, D. B., Delcarpio, J. B., Bahinski, A. and Izzo, N. J., Jr.** (1998). HL-1 cells: a cardiac muscle cell line that contracts and retains phenotypic characteristics of the adult cardiomyocyte. *Proc Natl Acad Sci U S A* **95**, 2979-2984.

**Consortium, E. P.** (2012). An integrated encyclopedia of DNA elements in the human genome. *Nature* **489**, 57-74.

**He, A., Kong, S. W., Ma, Q. and Pu, W. T.** (2011). Co-occupancy by multiple cardiac transcription factors identifies transcriptional enhancers active in heart. *Proc Natl Acad Sci U S A* **108**, 5632-5637.

**Liu, T., Ortiz, J. A., Taing, L., Meyer, C. A., Lee, B., Zhang, Y., Shin, H., Wong, S. S., Ma, J., Lei, Y., et al.** (2011). Cistrome: an integrative platform for transcriptional regulation studies. *Genome biology* **12**, R83.

**Thomas-Chollier, M., Defrance, M., Medina-Rivera, A., Sand, O., Herrmann, C., Thieffry, D. and van Helden, J.** (2011). RSAT 2011: regulatory sequence analysis tools. *Nucleic acids research* **39**, W86-91.

**Yang, G., Yuan, G., Ye, W., Cho, K. W. and Chen, Y.** (2014). An atypical canonical BMP signaling pathway regulates msh homeobox 1 (Msx1) expression during odontogenesis. *The Journal of biological chemistry*.

**Zhang, Y., Liu, T., Meyer, C. A., Eeckhoute, J., Johnson, D. S., Bernstein, B. E., Nusbaum, C., Myers, R. M., Brown, M., Li, W., et al.** (2008). Model-based analysis of ChIP-Seq (MACS). *Genome biology* **9**, R137.